Published online December 14, 2017

Special Section: Erosion and Lateral Surface Processes

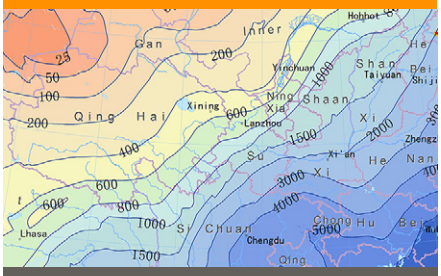

Core Ideas

- The *R* factor was developed in the various versions of the USLE.
- Research on rainfall erosivity estimation methods, mapping, and temporal trends is summarized.
- The RUSLE underestimates *R* factor values by about 10%.
- Three approaches for developing erosivity maps are identified.

S. Yin, X. Xue, State Key Lab. of Earth Surface Processes and Resource Ecology, Beijing Normal Univ., Beijing 100875, China, and School of Geography, Beijing Normal Univ., Beijing 100875, China; M.A. Nearing, USDA–ARS Southwest Watershed Research Center, Tucson, AZ 85719; P. Borrelli, Environmental Geosciences, Univ. of Basel, Basel, CH 4056, Switzerland. *Corresponding author (yinshuiqing@bnu.edu.cn).

Received 28 June 2017.
Accepted 27 Sept. 2017.

Citation: Yin, S., M.A. Nearing, P. Borrelli, and X. Xue. 2017. Rainfall erosivity: An overview of methodologies and applications. Vadose Zone J. 16(12). doi:10.2136/vzj2017.06.0131

Vol. 16, Iss. 12, 2017

Rainfall Erosivity: An Overview of Methodologies and Applications

Shuiqing Yin,* Mark A. Nearing, Pasquale Borrelli, and Xiaochan Xue

The rainfall erosivity factor (*R* factor) is one of six erosion factors in the Universal Soil Loss Equation (USLE), which together reflect the combined effects that cause soil loss by rill and interrill erosion on hillslopes by precipitation. It is defined as the summation of event EI_{30} (the product of kinetic energy and maximum 30-min intensity) over a year and calculated based on rainfall hyetograph data. The *R* factor was developed in the various versions of the USLE, including the definition of the individual event and the criterion for selecting events used in the calculation, the equation used to estimate the unit kinetic energy from the rainfall intensity, the estimation of erosivity from the snowmelt and thaw, and erosivity mapping. Most research on rainfall erosivity deals with any of three aspects: developing estimation methods for deriving erosivity from courser resolution rainfall data (such as daily, monthly, and annual) but with greater spatial and temporal coverages than those from hyetograph data; preparing erosivity maps including those for annual average, monthly, and 10-yr recurrence erosivity; and documenting temporal trends in erosivity. Rainfall erosivity research on these three aspects is summarized to provide a greater understanding of the *R* factor.

Abbreviations: KE, kinetic energy; MIT, minimum inter-event time; NWRR, Northwestern Wheat and Range Region; RUSLE, Revised Universal Soil Loss Equation; USLE, Universal Soil Loss Equation.

Soil erosion was recognized as a serious problem in the United States after the development and cultivation of new agricultural lands during the 1800s and early 1900s. In the late 1920s, a social consciousness campaign undertaken by the USDA, led by Hugh Hammond Bennett, helped to bring public attention to soil erosion as a "national menace." As a result of this effort, the US Congress appropriated money in 1930 to establish experimental erosion stations across primarily the eastern half of the country (Bennett, 1939). Bennett oversaw the establishment of 10 experiment stations utilizing methods developed by Miller (Bennett, 1939). That number increased ultimately to a total of 49 stations with natural runoff plots from which soil loss data were collected.

These and earlier observations and measurements provided valuable data to develop soil erosion prediction models. Zingg (1940) developed one of the earliest quantitatively based soil erosion prediction equations, which was related to the slope length and gradient. Smith (1941) and Browning et al. (1947) added soil erodibility, crop, and supporting-practice factors to the equation. The Musgrave equation was the first to include a rainfall erosivity factor in the process of soil erosion estimation (Musgrave, 1947). The rainfall erosivity factor was defined as a power-law function with the 2-yr, 30-min rainfall as the base number and 1.75 as the exponent. In the erosion equation proposed by Van Doren and Bartelli (1956), the rainfall factor was the intensity and frequency of 30-min rainfall. These rainfall factors performed satisfactorily at some locations, but were not adequate for use across the entire United States.

Wischmeier and Smith (1958) analyzed precipitation and soil loss data from fallow plots at three observation stations in Missouri, Iowa, and Wisconsin and identified that the event EI_{30}, the product value of total storm kinetic energy (E) and its maximum 30-min intensity (I_{30}), estimated the single storm soil erosion best. These EI_{30} values reflected

the combined potential effect of raindrop splash and runoff scour on soil erosion. The rainfall erosivity factor (*R* factor) is defined as the summation of the event EI_{30} values over a year. Wischmeier (1959) analyzed approximately 8000 plot-years of basic runoff, soil loss, and associated precipitation and related data in 21 states in the eastern part of the United States gathered by the National Runoff and Soil Loss Data Center from the erosion stations that were operating at that time. They confirmed the *R* factor's suitability at these locations, not only for fallow plots but also for continuous row crop plots, and not only for storm-to-storm variation but also for seasonal and yearly variations. The *R* factor became one of six factors in the Universal Soil Loss Equation (USLE, Wischmeier and Smith, 1965). The other five factors are the soil erodibility, slope length, slope steepness, cover-management practices, and support conservation practices. Wischmeier and Smith (1965) remarked: "One major difference between the Universal Soil Loss Equation (USLE) and its predecessors is in the manner and precision with which locational differences in rainfall are brought into the soil loss computations."

Development of the *R* Factor in New Versions of the USLE

The USLE (Wischmeier and Smith, 1965, 1978) and its two revised versions, RUSLE (Renard et al., 1997), and RUSLE2 (USDA–ARS, 2013), have been widely tested and implemented in the practice of soil and water conservation throughout much of the world. There are some differences in the rainfall erosivities among the different versions of the USLE and applications of the USLE and RUSLE in other countries and regions, including the definition of individual event and the criterion of an erosive event, the estimation of the unit kinetic energy from the intensity, the estimation of erosivity from snowmelt and thaw, the isoerodent map, etc. (Table 1).

Delineating the Individual Storm and the Criterion of the Erosive Storm

Continuous pluviographic data from recording rain gauges are composed of wet and dry periods. A storm was defined as the duration of rainfall with dry periods less than "minimum inter-event time" (MIT). The MIT in the USLE (Wischmeier and Smith, 1965, 1978) and RUSLE2 (USDA–ARS, 2013) was 6 h. The reason for this was that the best correlations of storm soil loss and EI_{30} values were obtained when the MIT was set to be 6 h (Wischmeier, 1959). There is a slight difference for the storm definition in the RUSLE, where a longer storm period is divided into two storms when there is <1.3 mm (0.05 inch) during the 6-h storm period.

Wischmeier and Smith (1978) defined an erosive storm as the rain shower with total rainfall amount no less than 12.7 mm (0.5 inch) or the one with a maximum 15-min intensity >25.4 mm h^{-1}. Analyses showed that the EI_{30} values for non-erosive storms were usually too small to generate runoff and soil loss, whereas the cost of dealing with the breakpoint data of these storms was high. Non-erosive storms and snow events were excluded prior to the calculations.

In the RUSLE (Renard et al., 1997), the same erosive threshold was used in calculating erosivity in the eastern, generally more humid, part of the United States, whereas all storms were used in the western, drier part of the country. Data for the Reynolds Creek watershed in southwestern Idaho (western United States) showed a 28 to 59% increase of EI_{30} values by including all storms in the calculation compared with including only erosive storms (Cooley et al., 1988). Using all storms with no threshold, erosivity showed an increase of 3.6% for the Goodwin Creek Watershed in northern Mississippi (eastern United States) (McGregor et al., 1995) and 1 to 10% with an average of 4.5% for 41 sites in the tropical region of Australia with annual rainfall varying from 261 to 4030 mm (Yu, 1999). Generally, in modern times with computers and digital data, the cost of using the "non-erosive" storms is trivial. This raises the question of whether storms with small rainfall amounts should still be excluded. We know that some storms above the threshold of the erosive storm may not result in measurable runoff and soil loss, whereas some below it may cause erosion. Xie et al. (2002) developed a practical method for identifying the threshold of an erosive storm, in which the EI_{30} values of the storms that generate runoff but are omitted from the calculation are balanced with the EI_{30} values of those that do not cause runoff but are included in the calculation. Rainfall and runoff data at an experimental station of the Yellow River Basin in China were used to obtain an erosive rainfall amount threshold of 12 mm, which is very similar to the threshold suggested in the USLE.

Non-rainfall precipitation events, rainfall events with amount <12.7 mm, and extreme events greater than a 50-yr storm (equal to or greater than a 100-yr storm) were excluded ahead of calculations for the RUSLE2. The reason for removing the extremes was to capture the main effects and for consistency so that farmers, contractors, and others are treated fairly when the RUSLE2 is used for conservation and erosion control planning in the United States. However, it is arguably best to include extreme events in the calculation of *R* for other erosion prediction applications, such as protecting highly sensitive water bodies and designing sediment storage in reservoirs, applications for which erosivity values developed for the RUSLE2 are not recommended (USDA–ARS, 2013).

Estimation of the Unit Kinetic Energy from the Intensity

Soil erosion processes are greatly dependent on the rainfall kinetic energy, which is a function of the size and fall-velocity of raindrops. Because the direct measurement of kinetic energy (KE) requires sophisticated and costly instruments, many different estimating

Table 1. Development of erosivity *R* factor in the new versions of the USLE.

Parameter	USLE (Wischmeier and Smith, 1965)	USLE (Wischmeier and Smith, 1978)	RUSLE (Renard et al., 1997)	RULSE2 (USDA–ARS, 2013)
Minimum inter-event time	no rainfall over 6 h	same as Wischmeier and Smith (1965)	<1.3 mm over 6 h	same as Wischmeier and Smith (1965)
Storms included	all storms	total rainfall amount ≥12.7 mm; or with $I_{15} \geq 25.4$ mm h^{-1}	East of Rocky Mountains: same as Wischmeier and Smith (1978); west of Rocky Mountains: all storms	total rainfall amount ≥12.7 mm and return level ≤50 yr
Kinetic energy–intensity equation	Eq. [1a]	Eq. [1a–1b]	Eq. [2]	Eq. [3]
Erosivity from snowmelt and thaw		Sub-factor R_s to the EI_{30} values for northwestern region based on Eq. [4]	equivalent *R* factor R_{eq} in the cropland areas of the NWRR† based on Eq. [5a–5b]	R_{eq} in the cropland areas of the NWRR based on Eq. [6]
Isoerodent maps	181 stations with breakpoint data plus 1700 stations with annual avg. precipitation, 2-yr, 1-h amount and 2-yr, 24-h amount for eastern part	same as Wischmeier and Smith (1965) for eastern part; using a relationship of $27.38P^{2.17}$, where *P* is the 2-yr, 6-h rainfall amount for western part	same as Wischmeier and Smith (1965) for eastern part; 790 stations with 60-min rainfall data for western part	Monthly erosivity density map from 3700 stations with 15-min data; PRISM monthly precipitation data with a resolution of 4 km multiplying density map to obtain monthly erosivity
Seasonal variation	12 monthly values, 33 climatic zones for eastern part	24 half-month values, 33 climatic zones for eastern part	24 half-month values, 120 zones in the contiguous United States	daily erosivity values disaggregated from monthly values and no zones divided

† NWRR, Northwestern Wheat and Range Region.

methods have been developed that incorporate rainfall intensity (*I*) using logarithmic, exponential, or power law formulations for kinetic energy–intensity (KE-*I*) relationships. Wischmeier and Smith (1958) first derived a logarithmic KE-*I* function based on the measurements of drop size distribution and terminal velocity observed at Washington, DC, by Laws and Parsons (1943), and it was used to estimate rainfall erosivity in the USLE (Wischmeier and Smith, 1965). Hudson (1963) and Carter et al. (1974) suggested that KE tends to reach a maximum value as *I* increases. In response to this research, Wischmeier and Smith (1978) suggested a limited constant value of 0.283 MJ ha^{-1} mm^{-1} for rainfall intensities (i_r) exceeding 76 mm h^{-1}:

$$e_r = 0.119 + 0.0873 \log_{10}(i_r), \quad i_r \leq 76 \text{ mm h}^{-1} \qquad [1a]$$

$$e_r = 0.283, \quad i_r > 76 \text{ mm h}^{-1} \qquad [1b]$$

where e_r is rainfall kinetic energy.

Kinnell (1981) suggested that an exponential model describes the KE-*I* relationship better than the logarithmic form, and this was confirmed by others (e.g., McGregor and Mutchler, 1976; Brown and Foster, 1987; van Dijk et al., 2002; Fornis et al., 2005). Brown and Foster (1987) recommended an exponential equation based on the work by Rosewell (1986) and suggested a maximum unit e_r of approximately 0.29 MJ ha^{-1} mm^{-1}; this was used in the RUSLE to estimate KE (Renard et al., 1997):

$$e_r = 0.29\left[1 - 0.72\exp\left(-0.05 i_r\right)\right] \qquad [2]$$

McGregor et al. (1995) compared the KE equations used in the USLE and RUSLE and noted that, for intensities between 1 and 35 mm h^{-1}, the results from the RUSLE were about 12% less than those predicted by the USLE. Both the USLE and RUSLE were compared with the results of the equation of McGregor and Mutchler (1976), which was developed based on 29 standard recording rain gauges in the Goodwin Creek Watershed in northern Mississippi. The results showed that the annual erosivities predicted by the equation of McGregor and Mutchler (1976) and the USLE were almost identical, whereas the RUSLE predicted values that were about 8% lower. McGregor et al. (1995) suggested that the equation of Brown and Foster (1987) be modified, changing the rate of increase of erosivity with rainfall intensity to 0.082 rather than the previous 0.05. The USDA–ARS (2013) used the 0.082 value in the RUSLE2:

$$e_r = 0.29\left[1 - 0.72\exp\left(-0.082 i_r\right)\right] \qquad [3]$$

The underestimation of unit energy in the RUSLE was also reported in Australia (Yu, 1999), Belgium (Verstraeten and Poesen, 2006), and Peninsular Malaysia (Shamshad et al., 2008). Six-minute precipitation data for 41 sites in the tropical region of Australia showed that the *R* factor using the RUSLE varied from 5.4 to 17%, with an average of 9.4%, lower than that using the USLE (Yu, 1999). A 105-yr 10-min rainfall depth time series for Ukkel, Brussels (Belgium), demonstrated that a 26% larger value of the *R* factor was obtained by using a local KE-*I* relationship compared with using the KE-*I* equation recommended in the RUSLE (Verstraeten and Poesen, 2006). Shamshad et al. (2008) also

showed that KE values calculated by the RUSLE were 8.4% less than those calculated using the equations of Onaga et al. (1988) in Peninsular Malaysia.

Analysis from 18 weather stations with 1-min precipitation data distributed across the central and eastern regions of China (the same data set used by Yin et al., 2015) showed that the behavior of the USLE was very similar to that of the RUSLE2 (the average deviation of the *R* factor for 18 stations is 0.4%). The RUSLE underestimated *R* factor values by about 9.3% (Table 2). The underestimation by the RUSLE seems to be more serious as the event KE values increase (Fig. 1 contains two examples). Result from 36 stations across Italy confirmed the conclusion on the underestimation of the RUSLE from the RUSLE2 (Table 3). The deviation of the USLE from the RUSLE2 based on data in Italy varied from 0.2 to 15.6% with a mean of 5.7%, which is greater than that based on data in China (Tables 2 and 3). The reason for the lower computed erosivity values for the RUSLE compared with the RUSLE2 is evident in the graph of unit rainfall energy vs. rainfall intensity (Nearing et al., 2017). The underestimation depends on the local dynamics of rainfall intensities.

Erosivity from Snowmelt and Thaw

The rainfall erosion index EI_{30} reflects the erosive forces of rainfall and its directly associated runoff. In some cold areas, erosion may be derived from the runoff associated with surface thaws and snowmelt, which was not taken into account in the first version of the USLE (Wischmeier and Smith, 1965). Wischmeier and Smith (1978) emphasized the importance of runoff on erosion and, from the "rainfall factor" in the 1965 version of the USLE, developed the "rainfall and runoff factor" in the 1978 version. Erosion by runoff from snowmelt, thaw, or light rain on frozen soil was taken into consideration using

$$R_s = 1.5P \quad [4]$$

where R_s is a sub-factor added to the EI_{30} values to obtain *R* in cold seasons, and *P* is the local December to March precipitation, measured as inches of water. This equation was developed in the northwestern region of the United States (Wischmeier and Smith, 1978). It was suggested that Eq. [4] also be applied in the northern tier of the central and eastern states, where runoff by snowmelt and thaw is thought to be a significant factor influencing soil erosion.

Renard et al. (1997), in developing the RUSLE, did not support the R_s method and ignored snowmelt and thaw erosivity in the areas outside the cropland areas of the Northwestern Wheat and Range Region (NWRR) due to insufficient research. An equivalent *R* factor, R_{eq}, was introduced in the cropland areas of the NWRR to reflect runoff from frozen and partially thawed soils:

Table 2. Comparison of *R* factor values from the USLE and RUSLE with those from the RUSLE2 for 18 stations from 1961 (1971) through 2000 across central and eastern regions of China.

Station	Location	Elevation	RUSLE2	Deviation of USLE	Deviation of RUSLE
		m	MJ mm ha^{-1} h^{-1} yr^{-1}	%	
Nenjiang	49.2° N, 125.2° E	243	1368.7	0.4	−9.5
Tonghe	46.0° N, 128.7° E	110	1632.5	0.1	−9.2
Wuzhai	38.9° N, 111.8° E	1402	781.9	2.6	−10.6
Yangcheng	35.5° N, 112.4° E	659	1503.3	0.9	−9.8
Suide	37.5° N, 110.2° E	929	992.8	1.1	−10.0
Yan'an	36.6° N, 109.5° E	959	1233.7	1.2	−9.2
Guanxiangtai	39.9° N, 116.3° E	55	3188.1	−1.6	−7.9
Miyun	40.4° N, 116.9° E	73	3575.0	−1.8	−7.8
Chengdu	30.7° N, 104.0° E	506	3977.0	−0.7	−8.9
Xichang	27.9° N, 102.3° E	1591	3021.0	2.0	−10.2
Suining	30.5° N, 105.6° E	280	4091.3	−0.8	−8.5
Neijiang	29.6° N, 105.1° E	352	5097.9	−1.1	−8.3
Fangxian	32.0° N, 110.8° E	427	2298.4	1.1	−8.5
Huangshi	30.3° N, 115.1° E	21	6049.4	0.1	−9.2
Tengchong	25.0° N, 98.5° E	1649	3648.9	2.3	−10.9
Kunming	25.0° N, 102.7° E	1897	3479.0	0.4	−9.7
Fuzhou	26.1° N, 119.3° E	84	5871.1	0.9	−9.4
Changting	25.9° N, 116.4° E	311	8258.5	0.0	−9.1
Avg.			2871.2	0.4	−9.3

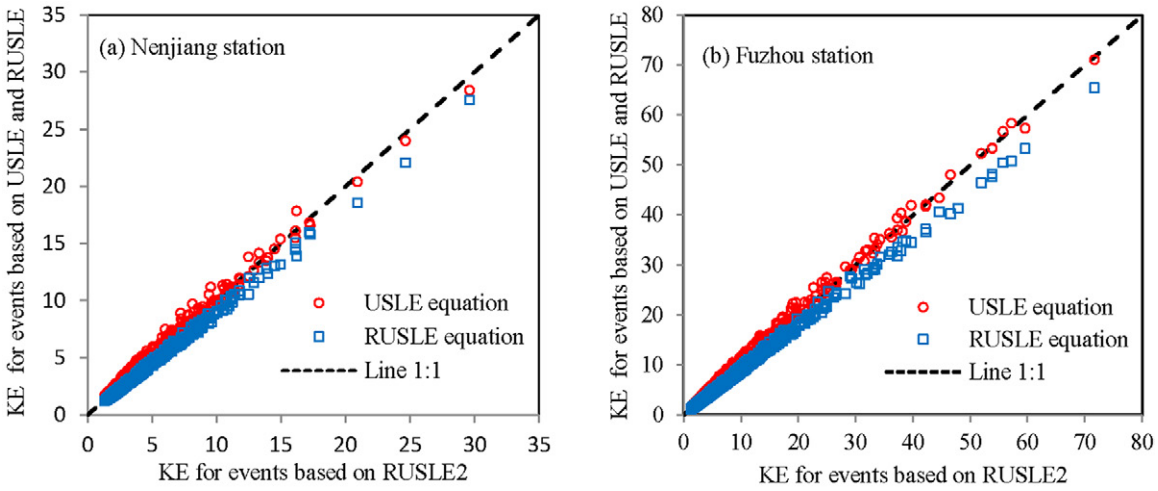

Fig. 1. Comparison of event kinetic energy (KE) among three versions of the Universal Soil Loss Equation model for (a) Nenjiang station and (b) Fuzhou station.

$$R_{eq} = -129.0 + 12.61P \quad [5a]$$

$$R_{eq} = 1.602\exp(0.2418P), \quad 7.5 < P < 15.0 \quad [5b]$$

where R_{eq} is the equivalent R factor in US erosivity units and P is the annual precipitation (inches). The maximum limit of the R_{eq} value is 320 US erosivity units because winter wheat (*Triticum aestivum* L.) is generally not grown where P is greater than about 89 cm (P = 35.6 in). Equation [5b] was suggested for use in areas of the NWRR with lower precipitation to smooth the transition across the boundary between the NWRR and non-NWRR and should be used for P < 38.1 cm (15.0 in).

Plot data for Pullman, WA, and Pendleton, OR, showed that the following equation works well in the NWRR (USDA–ARS, 2013):

$$R_{eq} = -50.5 + 7.86P \quad [6]$$

The maximum limit of R_{eq} was set to 200 US erosivity units (P = 81 cm [31.9 in]). To evaluate the difference between Eq. [4] and [5], we assumed that annual precipitation varies from 38 to 89 cm and obtained the relative deviation of the R_{eq} value for Eq. [6] for the RUSLE2 from that for Eq. [5a] for the RUSLE ranging from 12.1 to −28.1%.

Two aspects make the NWRR a unique area: (i) the temperature swings above and below freezing frequently and in a large amplitude throughout the winter months, which makes the soil change between freezing and thawing conditions repeatedly across the winter season; (ii) there is plentiful precipitation in the winter season, which results in a high probability of having rainfall and runoff on thawing soils that are vulnerable to erosion (McCool et al., 1995). The snowmelt and thaw effect on erosion was not considered in the erosivity for the northern tier of central and eastern states and is partially considered in the seasonal variation of the soil erodibility factor K for the RUSLE2 (USDA–ARS, 2013). Runoff on thawing soils is limited to about one month and the precipitation in that period is limited in these areas, which is different from the condition in the NWRR. Research conducted at Morris, MN, indicated that the erosion occurring during the spring thawing period composed approximately 7% of the annual erosion. More research on the snowmelt and thaw effect on erosion is needed.

Mapping Erosivity in the United States

To map erosivity for the USLE in the United States, rainfall erosivity values were computed at locations where continuous pluviographic data were available. Then the points with known rainfall erosivity values were used to estimate values at unknown points through spatial interpolation techniques. The isoerodent maps represented the first attempt to obtain spatial distributions of erosivity, with which rainfall erosivity information can be obtained at any location on the map with and without rainfall observations. Wischmeier (1962) developed regression relationships between R factors calculated from the breakpoint data with the product of three factors, including average annual rainfall, the 2-yr, 1-h amount, and the 2-yr, 24-h amount, which were more widely available than the breakpoint data. The relationships made it possible for average annual rainfall and the published and unpublished rainfall intensity–frequency data for 1700 stations to be included in the generation of the isoerodent map for east of the Rocky Mountains in the United States as a supplement to information for the available 181 stations with 22 yr (1936–1957) of breakpoint data (Wischmeier and Smith, 1965). The isoerodent map was later extended to the Pacific Coast using a relationship of $27.38P^{2.17}$, where P is the 2-yr, 6-h rainfall amount (Wischmeier and Smith, 1978). The RUSLE updated the map for the eastern part of the United States using corrections and a more refined smoothing technique and included more precise R values for the western part of the United States by including 790 stations with 60-min rainfall data (Renard et al., 1997). The regional conversion

Table 3. Comparison of *R* factor values from the USLE and RUSLE with those from the RUSLE2 for 36 stations across Italy from 2002 through 2011.

Station	Location	Elevation	RUSLE2	Deviation for USLE	Deviation for RUSLE
		m	MJ mm ha^{-1} h^{-1} yr^{-1}	%	
Alpe Devero	46.3° N, 8.3° W	1634	1439.8	13.3	−13.0
Altamura	40.9° N, 16.4° W	512	1231.0	1.3	−11.4
Amatrice	42.6° N, 13.3° W	905	787.1	11.2	−12.8
Apricena	41.8° N, 15.4° W	51	1660.3	2.8	−11.0
Ardea	41.6° N, 12.5° W	47	1819.2	2.4	−10.5
Ariano Irpino	41.2° N, 15.1° W	678	1320.7	2.6	−11.0
Asola	45.2° N, 10.4° W	41	1270.5	4.9	−11.3
Bellosguardo	40.4° N, 15.3° W	554	1687.3	8.0	−12.5
Bettola	44.8° N, 9.6° W	600	1468.9	6.9	−11.4
Bomba	42.0° N, 14.4° W	457	2018.8	4.3	−11.0
Botricello	38.9° N, 16.9° W	18	2211.8	1.4	−10.9
Carpegna	43.8° N, 12.3° W	792	1431.0	8.0	−12.1
Casamazzagno	46.6° N, 12.5° W	1341	1433.5	9.1	−12.6
Casole dElsa	43.3° N, 11.0° W	418	1519.5	4.5	−11.1
Courmayeur- Ferrache	45.9° N, 7.0° W	2290	594.6	15.5	−13.0
Diga del Chiotas	44.2° N, 7.3° W	2020	1751.6	13.6	−13.7
Enna	37.6° N, 14.3° W	950	1293.8	3.5	−12.7
Fasano	40.8° N, 17.5° W	64	1447.1	2.2	−10.8
Fondi	41.3° N, 13.4° W	5	2446.3	3.3	−11.1
L'Aquila	42.3° N, 13.4° W	596	435.9	10.1	−12.0
Massa Lubrense	40.6° N, 14.4° W	385	3012.2	2.3	−11.0
Monte Castellino	44.3° N, 10.4° W	887	2080.9	9.3	−12.6
Muravera	39.4° N, 9.6° W	15	1416.1	4.1	−12.4
Nociglia	40.0° N, 18.3° W	95	2200.4	2.4	−11.9
Oga Colombano	46.5° N, 10.3° W	2300	647.7	15.6	−13.8
Osimo	43.5° N, 13.5° W	115	1305.5	3.4	−9.6
Pareto	44.5° N, 8.4° W	525	1504.9	8.3	−12.8
Perugia	43.1° N, 12.4° W	330	1436.1	3.0	−11.6
Pradon Porto Tolle	44.9° N, 12.4° W	−3	2241.3	0.2	−9.8
Rizziconi-Ponte Vecchio	38.4° N, 15.9° W	30	2373.5	3.2	−11.3
Roseto Capo Spulico	40.0° N, 16.6° W	151	1150.2	3.6	−11.8
S. Volfango	46.2° N, 13.6° W	650	5072.2	5.0	−12.1
Tuscania	42.4° N, 11.9° W	165	1703.6	4.7	−12.0
Valledoria	40.9° N, 8.8° W	20	822.0	4.4	−12.4
Vercelli	45.4° N, 8.4° W	132	1702.7	4.4	−10.7
Volpago del Montello	45.8° N, 12.1° W	125	3409.0	3.6	−10.8
Avg.			1704.1	5.7	−11.7

factors (ranging 1.08–3.16) between EI_{30} values calculated from the 15-min and 60-min data were used. The conversion factor of 1.0667 (Weiss, 1964) between those from the 15-min data and breakpoint data were used to account for the fact that maximum intensity values from the 15-min precipitation data are lower than those computed from the breakpoint rainfall.

The RUSLE2 used the precipitation data from the 1960s through 1999 and introduced an erosivity density, which is the ratio of monthly erosivity to monthly precipitation. Monthly erosivity density was calculated using 15-min precipitation data based on a conversion factor of 1.034 (Hollinger et al., 2002) between EI_{30} values from 15-min data and breakpoint data, which was slightly different from 1.0667 for the RUSLE. Note that monthly erosivity and monthly precipitation used to determine the monthly erosivity density were calculated based on the same 15-min data set because the essential meaning of erosivity density is to reflect the erosivity generated by a unit rainfall amount. Monthly erosivity density was mapped throughout the continental United States and was multiplied by more widely available monthly precipitation data sets (such as PRISM data from a 4-km grid, Daly et al., 1997) to obtain monthly erosivity. Note that monthly precipitation includes rainfall and snow. The annual erosivity is computed as the sum of the monthly erosivity values.

The USDA–ARS (2013) discussed the reasons for introducing erosivity density:

1. Daily precipitation data measured by simple rain gauges are more reliable and have fewer missing data than the 15-min precipitation data measured by weighing-bucket rain gauges. The ratio of the precipitation amounts for the 15-min data set to those for the daily data set for the same location ranged from 0.76 to 0.94. The RUSLE2 used the 15-min data to compute a ratio of erosivity to precipitation amount (erosivity density), rather than the absolute sum of erosivity used in the former editions, which was believed to be less influenced by the quality of the 15-min data. Analysis showed that the calculation of erosivity density values has a lower data requirement, in terms of requiring shorter record lengths and allowing more missing data in the record, compared with the direct calculation of annual erosivity values in the former versions.

2. More stations with daily rainfall observations could be used in the generation of isoerodent maps. There were approximately 3700 stations with 15-min records, 6400 with hourly records, and 12,800 with daily records in the United States from the 1970s through the end of the century (Hollinger et al., 2002). The introduction of the erosivity density method allowed the use of many more stations with daily records to be used to improve the spatial interpolation accuracy of the map.

3. Erosivity density is independent of the elevation up to about 3000 m, which means that erosivity density could be mapped for the entire continental United States rather than being separated into eastern and western parts as in the former versions.

Monthly distributions of EI_{30} (12 values) were required to derive the cover-management factor (C) to reflect the seasonal interactions of the cropping system and rainfall distribution. Based on these results, 33 climatic zones were divided into the area east of the Rocky Mountains in the USLE (Wischmeier and Smith, 1965). Half-monthly distribution (24 values) of EI_{30} was required for the soil erodibility factor (K) and C, and hence 120 zones were delineated in the contiguous United States for the RUSLE (Renard et al., 1997). The temporal erosivity distribution is assumed to be constant within a zone. Two locations with short distances across the zone boundaries may have a different zonal seasonal erosivity distribution, which may result in a large difference in estimated erosion for these two nearby stations. Hence, daily erosivity values (365 values) were disaggregated from the monthly values and no zones were divided in the RUSLE2, which allowed erosion estimates to distribute smoothly across the United States.

The 10-yr-frequency event EI_{30} value, which has the probability of occurring once every 10 yr, is useful in the runoff calculation for the contouring factor and for quantifying the effect of water ponding on reducing raindrop splash on flat and ridged surfaces. An extreme value distribution such as lognormal (Wischmeier and Smith, 1978) or the generalized extreme value (Hollinger et al., 2002) was used to fit annual maximum EI_{30} series and generate the 10-yr-frequency event EI_{30} for the USLE and RUSLE. To ensure enough samples to fit the distribution, a minimum of 20 to 25 yr of data is required. The RUSLE2 retained this method; however, it recommended inputting the 10-yr, 24-h rainfall (P_{10y24h}) to compute a corresponding 10-yr, 24-h EI_{30} (EI_{10y24h}) based on the relationship of $EI_{10y24h} = 2\alpha_m P_{10y24h}$, where α_m is the greatest monthly erosivity density value.

Estimation of Erosivity

As pointed out by Agnese et al. (2006), the ideal data for at-site estimation of erosivity is high temporal resolution data, such as hyetograph data (Yin et al., 2007; Bonilla and Vidal, 2011), 1-min (Yin et al., 2015; Xie et al., 2016), 5-min (Fiener et al., 2013), 6-min (Yu, 1998; Lu and Yu, 2002), 10-min (Verstraeten and Poesen, 2006; Meusburger et al., 2012; Shiono et al., 2013; Ma et al., 2014), 15-min (USDA–ARS, 2013; Angulo-Martinez and Beguería, 2012; Klik and Konecny, 2013; Klik et al., 2015), 20-min (Capolongo et al., 2008), 30-min (Panagos et al., 2015, 2016b), and 60-min (Renard et al., 1997) interval data. Conversion factors are generally used to adjust the R factor based on the different intervals of rain data to that based on the hyetograph data (Yin et al., 2007; Panagos et al., 2016a; Porto, 2016). However, there are fewer recording rain gauges with higher time resolution, and the high-resolution data tend to have greater rates of missing data and shorter record lengths. Recall that one reason why the RUSLE2 (USDA–ARS, 2013) calculated the ratio (erosivity density) of erosivity to the precipitation using 15-min data instead of the sum of EI_{30} in the former versions is the relatively greater rate of missing data in the 15-min records (Hollinger et al., 2002).

A general technique used for erosivity estimation is to develop simple empirical relationships between erosivity from limited finer resolution data and coarse-resolution rainfall, such as daily, monthly, and

annual rainfall, and then to extend the relationship to wider areas with coarser temporal resolution rainfall data. For example, Yin et al. (2015) developed and calibrated 21 models based on rainfall data collected across a range of temporal resolutions in the eastern half of China and recommended 17 of them for developing erosivity maps when different coarser resolution data are available in the study area. It was also reported that finer resolution data generated better estimations of erosivity at a given output timescale. Models using daily rainfall data were often used because daily-scale rainfall data collected from simple rain gauges are relatively common and they can satisfy the three usage requirements in the USLE, which is the average annual rainfall erosivity for predicting average annual soil loss, the seasonal distribution curve of rainfall erosivity reflecting the interactions of the cropping system management and rainfall seasonal distributions, and the 10-yr event or daily rainfall erosivity for assessing the effect of ponding on rainfall erosivity and the effectiveness of the terrace practice. A simple power law form of the Richardson model (Richardson et al., 1983), combined with a sinusoidal or co-sinusoidal function reflecting the annual cycle of the coefficient of the power law function (Yu and Rosewell, 1996; Yu, 1998; Yu et al., 2001; Capolongo et al., 2008; Zhu and Yu, 2015; Xie et al., 2016) was recommended in a comparison study conducted by Angulo-Martinez and Beguería (2009) when estimating the annual average and seasonal distribution of rainfall erosivity values. However, a combination of daily rainfall amount and daily maximum 60-min rainfall significantly improved predictions of the daily erosivity index, and sub-daily data were recommended to be used when estimating daily erosivity values (Xie et al., 2016). Xie et al. (2016) assessed parameters for empirical models estimating *R* from daily rainfall data developed in other parts of the world (Richardson et al., 1983; Yu, 1998; Yu et al., 2001) to determine if they can be adopted in China without calibration. The result demonstrated that parameters from Yu (1998) produced a reasonable result, whereas those from the other two studies overestimated *R* seriously, which indicated that the parameters should be calibrated based on high temporal resolution rainfall records before they are extrapolated to a different climate zone (Oliveira et al., 2012b; Xie et al., 2016).

Also, satellite-based and radar-based precipitation data are especially useful in areas with sparse distributions of rain gauges, such as in Africa (Vrieling et al., 2010, 2014) and Tibet (Fan and Yang, 2013). High-resolution rainfall data at gauging stations are needed to validate the erosivity obtained from satellite-based precipitation products.

Mapping Outside the United States

The latest UN Status of the World's Soil Resources report highlighted that "...the majority of the world's soil resources are in only fair, poor or very poor condition" (FAO, 2015). The USLE-based models are the most widely used soil erosion assessment tools outside the United States. Mapping rainfall erosivity (the *R* factor) at regional or larger scales represents an important step to assess soil loss by water erosion and helps to gain a better understanding of its spatial patterns.

Recent development of geospatial technologies has facilitated the development of new regression techniques to compute spatially continuous maps of rainfall erosivity. Literature insights indicated three approaches to perform spatial interpolation of rainfall erosivity. The first one is the generalization of model parameters. Lu and Yu (2002) used a daily erosivity model to generate a rainfall erosivity map in Australia. Two parameters of the model were set to be constant for the study area and another parameter was related to the ratio of the mean summer rainfall to the mean annual rainfall. Yang and Yu (2015) indicated that the parameters of Lu and Yu (2002) may change with the period of reference and improved the model by using the geographic location and elevation to predict the parameters instead of rainfall. The second one is to estimate the at-site rainfall erosivity with observations first and then interpolate erosivity values for the sites without observations by geostatistical techniques such as inverse distance weighting (Sadeghi et al., 2017), ordinary kriging (Oliveira et al., 2012a), co-kriging (Qin et al., 2016), regression kriging (Meusburger et al., 2012; Borrelli et al., 2016), or Gaussian process regression (Panagos et al., 2015). Geographical location, elevation, annual rainfall, and topography are usually used as covariates in the smoothing process (Goovaerts, 1999; Naipal et al., 2015). For example, Yin et al. (2013) collected erosive daily rainfall (daily rainfall amount $\geq$10 mm) from 2678 weather and hydrologic stations from 1981 through 2010 and generated an *R* factor raster map across mainland China (Fig. 2) for the purpose of soil erosion assessment in the fourth census on soil erosion across China (Liu et al., 2013). Panagos et al. (2015) developed an erosivity raster map at 1-km resolution for Europe based on 1541 stations with 5- to 60-min interval data and a Gaussian process regression interpolation method with climatic indices (total precipitation, seasonal precipitation, precipitation of the driest and wettest months, average temperature), elevation, and latitude and/or longitude as covariates (Fig. 3). The third interpolation approach is to use available gridded precipitation data to generate *R* factor and erosivity density maps (Zhu and Yu, 2015; Panagos et al., 2015, 2016b). For example, Panagos et al. (2015) used a generated *R* factor raster map and 1-km resolution of monthly averages of precipitation from the WorldClim data set (Hijmans et al., 2005) to map erosivity density for Europe.

A wide range of studies on generating a continuous spatial representation of rainfall erosivity has been presented in the international scientific literature. Gathering information from Scopus and Google Scholar databases, 51 studies on the mapping of rainfall erosivity outside of the United States were collected and summarized (Table 3). The study areas range from 200 km^2 (Men et al., 2008) to a global scale (Naipal et al., 2015; Panagos et al., 2017b). The vast majority of the interpolations were performed through kriging (simple, ordinary, and universal, 24

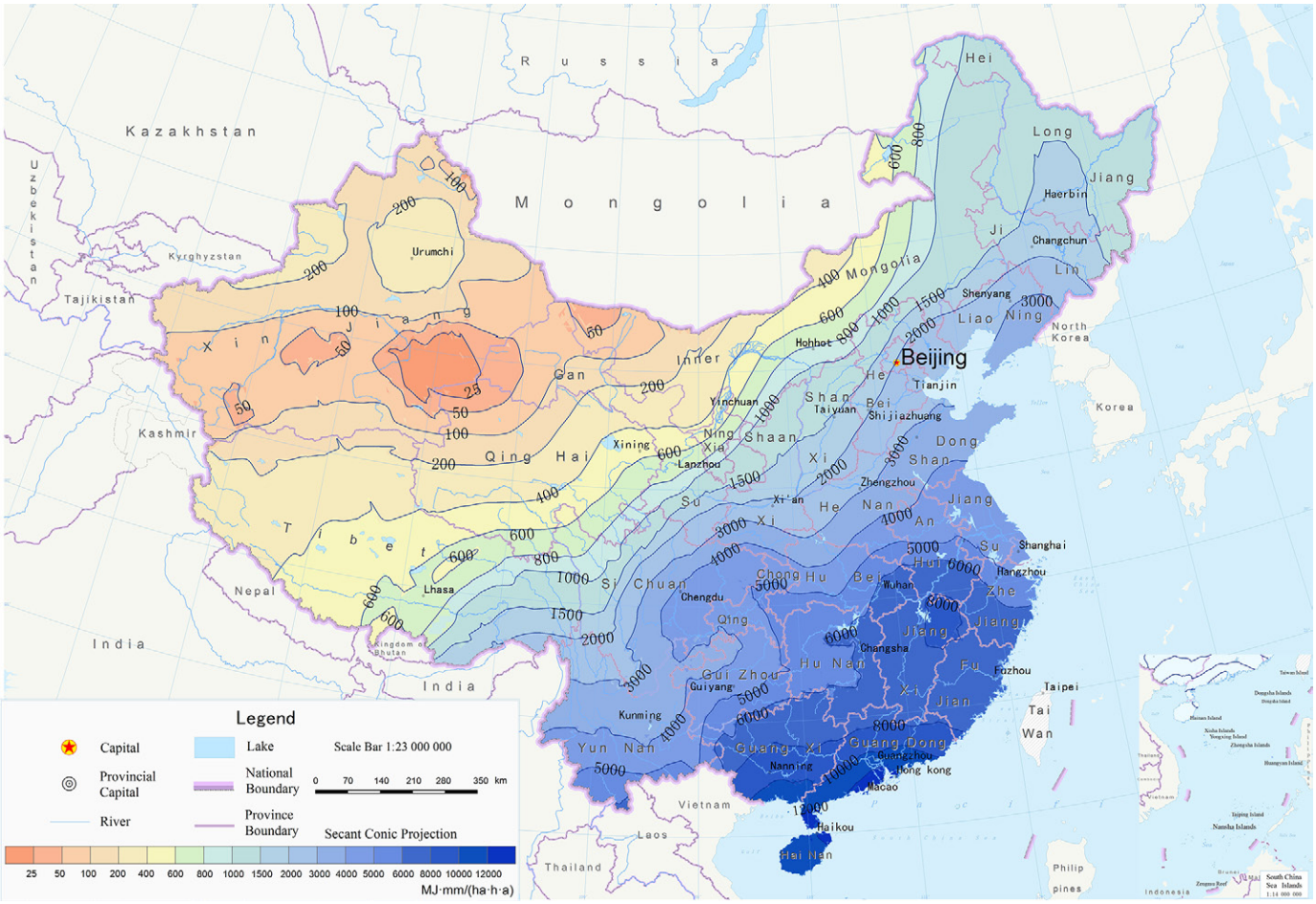

Fig. 2. Rainfall erosivity map for mainland China (data source: Yin et al., 2013).

studies) and deterministic interpolation methods such as inverse distance weighting (11 studies). Hanel et al. (2016) compared the spatial interpolation models for rainfall erosivity in the Czech Republic that included inverse distance weighting, simple kriging, ordinary kriging, simple co-kriging, ordinary co-kriging, regression kriging, and generalized least squares and reported that the spatial interpolation models that included long-term rainfall characteristics as the covariates (regression kriging and generalized least squares) performed considerably better than those based on local interpolation and/or geographical information only (inverse distance weighting, simple kriging, ordinary kriging, simple co-kriging, and ordinary co-kriging) in the study area. Some of the studies performed with the interpolation techniques of kriging and inverse distance weighting also presented monthly or seasonal rainfall erosivity maps as well as annual average erosivity maps (Lu and Yu, 2002; Shamshad et al., 2008; Sadeghi et al., 2011, 2017; Klik et al., 2015). Interpolation including the use of covariates represented approximately 20% of the observations, mostly realized through regression kriging (Meusburger et al., 2012; Borrelli et al., 2016; Schmidt et al., 2016), Gaussian process regression (Panagos et al., 2015, 2017b), generalized additive model (Panagos et al., 2016a; Laceby et al., 2016), and Cubist regression trees (Ballabio et al., 2017).

Monthly interpolations involving the use of covariates were performed in three studies. In Greece, Panagos et al. (2016b) spatially interpolated monthly rainfall erosivity values (30-min data for 80 stations covering about 30 yr) through a generalized additive model with average monthly rainfall, elevation, longitude, and latitude as the covariates. Schmidt et al. (2016) calculated at-site rainfall erosivity for 87 stations with 10-min rainfall data across Switzerland and generated 12 monthly rainfall erosivity maps with high spatial resolution for Switzerland based on a stepwise generalized linear regression method and high spatial resolution of precipitation and topography information as covariates. Ballabio et al. (2017) investigated the monthly variation of rainfall erosivity in Europe based on 1568 rainfall stations with high-resolution rainfall data in the Rainfall Erosivity Database at European Scale (REDES). A Cubist regression tree interpolation technique was used to estimate monthly values of rainfall erosivity across Europe, while the seasonal patterns were analyzed using a clustering algorithm technique. The covariates used were average monthly precipitation, average minimum and maximum monthly precipitation, average monthly temperature, and bioclimatic variables. Panagos et al. (2017b) used the new Global Rainfall Erosivity Database (GloREDa) to develop the first high-temporal-resolution global erosivity map. The global map with a 30-arcsec spatial resolution

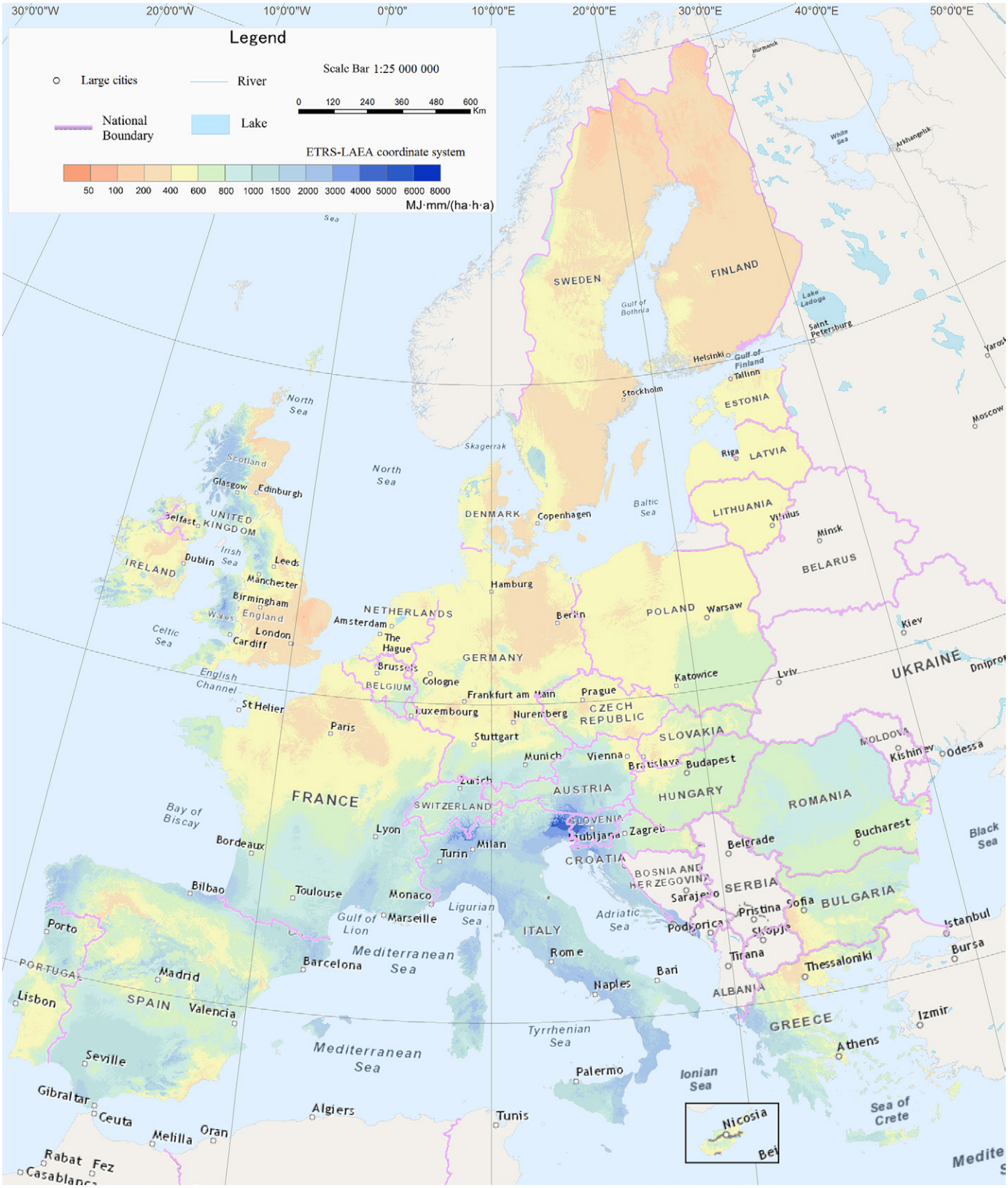

Fig. 3. Rainfall erosivity map for Europe (data source: Panagos et al., 2015).

was interpolated using a Gaussian process regression model. Input data were a time series of pluviographic records (hourly and sub-hourly) for 3625 stations covering 63 countries and a series of independent climatic covariates. The values of the global rainfall erosivity map range from 0 (Taklamakan Desert, China) to

>20,000 MJ mm ha^{-1} h^{-1} yr^{-1} (Costa Rica and Mauritius), with an average of 2190 MJ mm ha^{-1} h^{-1} yr^{-1}.

It is important to quantify the uncertainty and generate the uncertainty map as well as the *R* factor map. Five key sources of uncertainty in a rainfall erosivity map were evaluated including: (i) rainfall measurement limitations (instrumental errors), (ii) the efficiency of the KE-*I* equation used to compute rainfall kinetic energy from intensity, (iii) the effectiveness of the regressions used to compute rainfall erosivity from daily or coarser temporal resolution rainfall inputs, (iv) the interannual variability of annual rainfall erosivity values, and (v) the spatial variability of rainfall erosivity values (Catari et al., 2011; Hanel et al., 2016). The estimation of the spatial variability of rainfall erosivity values is mainly related to station density or the resolution of gridded data and the interpolation method used, including the effectiveness of the covariates (Table 4). Lu and Yu (2002) generated a rainfall erosivity map for Australia with gridded daily data. They used 132 sites with rainfall erosivity values compiled from previous investigations and 43 sites with values calculated from long-term 6-min rainfall data to assess the generated *R* factor map. The performances of the spatial interpolation models were evaluated by the leave-one-out or 10-fold cross-validation method (Borrelli et al., 2016; Panagos et al., 2017b). It is a pity that there has been little research reporting an uncertainty map of the *R* factor.

Long-Term Trends in Rainfall Erosivity

The probability of heavy rainstorms occurring in many mid-latitude regions has shown an increasing trend in recent decades, associated with a more active hydrological cycle due to increasing global surface temperatures (IPCC, 2013). Projection of precipitation extremes from eight high-resolution global climate models showed a significant intensification of daily extremes in the middle- and high-latitude areas of both hemispheres for the 21st century with low intermodal variability (Toreti et al., 2013). Temporal variations of the *R* factor, along with changes in the other soil erosion factors, reflect apparent temporal trends in the rates of soil erosion, which have significant implications for climate change impact assessment and mitigation. Studies on temporal variations of the *R* factor have been extensively reported based on historical records (Diodato and Bellocchi, 2009; Meusburger et al., 2012; Klik and Konecny, 2013; Ramos and Duran, 2014; Panagos et al., 2016a; Qin et al., 2016; Wang et al., 2017) and future climate projections (Nearing, 2001; Zhang et al., 2010; Shiono et al., 2013; Segura et al., 2014; Yang et al., 2015; Panagos et al., 2017a). Similar to the development of an erosivity map, high-temporal-resolution data usually cover limited stations and record lengths (Verstraeten and Poesen, 2006; Fiener et al., 2013), so most research in the past was based on the empirical relationship between erosivity values from high-resolution data and those from coarse-resolution rainfall (Angulo-Martinez and Beguería, 2012; Ma et al., 2014; Ramos and Duran, 2014). Long-term trends were reflected by erosivity values estimated from the empirical relationship assuming the parameters of the regressions did not change. Projections of erosivity were usually based on the coarse spatial and temporal resolution precipitation data simulated by the general circulation model under different emission scenarios and combined with spatial-temporal downscaling techniques (Zhang et al., 2010, 2012). Recently, Nearing et al. (2015) demonstrated that no trends in annual erosivity had been found in the historical records in a semiarid watershed of the American Southwest, whereas Zhang et al. (2012) reported significant increasing trends in annual erosivity in the downscaled projected general circulation model products existing in the same watershed, although no significant trends in the overall annual rainfall amounts had been detected. Further investigation into the downscaling techniques was suggested.

Because the climate is changing, maps and other information should be periodically updated. The *R* values across the United States in the USLE and for the eastern United States in the RUSLE were computed using data from approximately 1936 through 1957. Those for the western United States in the RUSLE were based on the period of 1971 through 1983. The RUSLE2 updated the erosivity map using precipitation data from the 1960s through 1999 due to the possible increasing rainfall amounts and intensities during the last 70 yr. About 10% greater values were demonstrated across much of the eastern United States compared with those for the 1936 through 1957 period. Note that the difference of 10% came from not only the precipitation change but also the analysis procedures discussed above, such as the alteration of the KE-*I* equation, the introduction of the erosivity density method, and so on.

Conclusion

In this study, we reviewed the evolution of erosivity prediction equations, the development of erosivity in the revised versions of the USLE, the erosivity estimation methods from daily or coarser resolution data, and spatiotemporal variations in erosivity. Analysis from 18 stations with 1-min rainfall data from China and 36 stations with breakpoint data from Italy consolidated the results from previous research that the RUSLE underestimated *R* factor values by about 10%. The concept of erosivity density introduced in the RUSLE2, describing the erosivity generated by a unit rainfall amount, improved the mapping of rainfall erosivity in the United States. Three approaches for developing erosivity maps were identified as the generalization of model parameters, interpolation of at-site rainfall erosivity, and the use of readily available gridded precipitation data to generate *R* factor maps. About half of the studies from the Scopus and Google Scholar databases used geostatistical interpolation techniques such as kriging, and one quarter of the studies used the deterministic interpolation technique of inverse distance weighting to generating erosivity maps based on the analysis of 51 studies from the United States using spatial interpolation techniques. Geographical location, elevation,

Table 4. Studies mapping rainfall erosivity outside the United States.

Country	Geographic location	Area	Stations with sub-hourly and hourly records†	Stations or grid resolution for interpolation	Station density or data resolution‡	Data type for *R* computation§	Interpolation method	Reference
		1000 km^2			km^2/station			
Algeria	northern Algeria	381	91	273	1396	monthly	regression kriging	Meddi et al. (2016)
Australia	New South Wales, South Australia	1788	0	128	13,969	annual	kriging	Ferro et al. (1991)
Australia	nationwide	7617.9	43	gridded data	0.05°‡	daily	ordinary kriging	Lu and Yu (2002)
Austria	Upper and Lower Austria	32.2	51	51	631	sub-hourly	kriging	Klik and Konecny (2013)
Belgium	nationwide	30.5	1	gridded data	0.5°	annual	inverse distance weighting	Diodato et al. (2014)
Brazil	Mato Grosso do Sul	358.2	3	109	3286	annual	ordinary kriging	Oliveira et al. (2012a)
Brazil	nationwide	8515.8	54	773	11,017	annual	multivariate linear models, ordinary kriging	Mello et al. (2013)
Chile	central Chile	NA¶	16	257	NA	annual	kriging	Bonilla and Vidal (2011)
China	Hebei Province	0.2	0	373	1	monthly	kriging and inverse distance weighting	Men et al. (2008)
China	Loess Plateau	640	0	87	7356	daily	inverse distance weighting	Xin et al. (2011)
China	nationwide	9600	18	2678	3585	daily	kriging	Yin et al. (2013)
China	Kejie catchment	1.8	6	12	150	daily	co-kriging	Ma et al. (2014)
China	dryland region	5580	92	390	14,308	daily	quadratic polynomial equation	Yang and Lu (2015)
China	nationwide	9600	0	756	12,698	daily	universal co-kriging	Qin et al. (2016)
Colombia	central Cordillera	1.4	6	16	88	seasonal	inverse distance weighting and local polynomial regression	Hoyos et al. (2005)
Cyprus	southern part	5.9	35	35	169	sub-hourly	generalized additive model	Karydas et al. (2015)
Czech Republic	nationwide	78.9	106	106	744	sub-hourly	empirical Bayesian kriging	Krása et al. (2014)
Czech Republic	Nationwide	78.9	96	gridded covariates	1 km	altitude, latitude, mean precipitation, and mean fraction of precipitation >95% quantile of monthly precipitation	generalized least-squares	Hanel et al. (2016)
Europe	EU-28	4475.8	1541	gridded covariates	1 km	climatic data, elevation, and latitude/longitude	Gaussian process regression	Panagos et al. (2015)
Europe	EU-28	4475.8	1675	gridded covariates	1 km	precipitation and temperature	Gaussian process regression	Panagos et al. (2017a)
Europe	EU-28	4475.8	1568	gridded covariates	1 km	monthly precipitation, monthly temperature, and bioclimatic variables	Cubist regression trees	Ballabio et al. (2017)
Greece	nationwide	132	80	gridded covariates	1 km	avg. monthly precipitation, elevation, and latitude/longitude	generalized additive model	Panagos et al. (2016a)

Continued on next page.

Table 4 continued from previous page.

Country	Geographic location	Area	Stations with sub-hourly and hourly records†	Stations or grid resolution for interpolation	Station density or data resolution‡	Data type for *R* computation§	Interpolation method	Reference
Honduras	nationwide	112	NA	344	326	annual	inverse distance weighting	Mikhailova et al. (1997)
Hungary	nationwide	93	4	Gridded covariate	23,250	elevation	kriging	Mezősi and Bata (2016)
Italy	Sicily	25.8	41	169	153	annual	kriging	Ferro et al. (1991)
Italy	Apulia, Basilicata, Calabria, Campania, Sicily	83.8	0	629	133	annual	kriging	Ferro et al. (1991)
Italy	Calabria	15.1	0	214	71	annual	kriging	Aronica and Ferro (1997)
Italy	nationwide	301.1	0	47	6406	monthly	thin plate spline	Van der Knijff et al. (1999)
Italy	Sicily	25.8	0	112	230	annual	universal kriging	Grauso et al. (2010)
Italy	Campania	NA	0	62	NA	annual	ordinary kriging	Fagnano et al. (2012)
Italy	nationwide	301.3	386	gridded covariates	1 km	elevation, annual rainfall, avg. temperature of the coldest quarter, isothermality, temperature seasonality, max. temperature of the warmest month, and precipitation of the coldest quarter	regression kriging	Borrelli et al. (2016)
Italy	Calabria	15.1	65	65	232	sub-hourly	kriging	Porto (2016)
Iran	nationwide	1874	18	18	104,111	sub-hourly	inverse distance weighting	Sadeghi et al. (2011)
Iran	nationwide	1874	70	70	26,771	sub-hourly	inverse distance weighting	Sadeghi et al. (2017)
Japan	Fukushima Prefecture	5.2	42	gridded covariates	0.25 km	rainfall, temperature, morphometric attributes, and distance to Pacific Ocean coast	generalized additive model	Laceby et al. (2016)
Jordan	North Jordan	3.7	NA	18	206	avg. annual	N/A	Eltaif et al. (2010)
Kenya	Nzoia catchment	12.7	0	14	907	avg. annual or monthly	inverse distance weighting, Thiessen polygon	Moses (2017)
Malaysia	Pulau Penang State	1	6	22	167	daily or annual	inverse distance weighting	Shamshad et al. (2008)
Mexico	Zenzontla	NA	0	30	NA	annual	inverse distance weighting	Millward and Mersey (1999)
Mexico	northwestern Mexico	NA	11	11	NA	sub-hourly	kriging	Norzagaray-Campos et al. (2016)
New Zealand	nationwide	268	35	597	449	average annual	universal kriging	Klik et al. (2015)
Nigeria	nationwide	923.8	0	17	54,341	daily	NA	Salako (2010)
Portugal	Algarve region	5	0	36	139	daily	kriging and co-kriging	Goovaerts (1999)
South Korea	nationwide	100.2	75	75	1336	sub-hourly	inverse distance weighting	Risal et al. (2016)
Spain	Ebro Basin	85	111	111	766	daily/annual	smoothing splines	Angulo-Martínez and Beguería (2009)

Continued on next page.

Table 4 continued from previous page.

Country	Geographic location	Area	Stations with sub-hourly and hourly records†	Stations or grid resolution for interpolation	Station density or data resolution‡	Data type for *R* computation§	Interpolation method	Reference
Spain	northeast	160	45	459	349	daily	linear regression and local autoregressive component	Beguería et al. (2009)
Switzerland	nationwide	41.3	71	gridded covariates	NA	elevation, aspect, latitude, longitude, avg. annual precipitation, and main biogeographic units	regression kriging	Meusburger et al. (2012
Switzerland	nationwide	41.3	87	gridded covariates	NA	precipitation and topography	regression kriging	Schmidt et al. (2016
Taiwan	Kaohsiung City and Pingtung County	5.7	55	55	104	sub-hourly	kriging	Lee and Lin (2015)
World	planet's land surface	NA	0	gridded data	0.5 and 0.25°	annual	linear multiple regression	Naipal et al. (2015)
World	planet's land surface	NA	3625	gridded covariates	1 km	avg. monthly precipitation, avg. min. and max. monthly precipitation, avg. monthly temperature, precipitation of the wettest and driest months, and precipitation seasonality	Gaussian process regression	Panagos et al. (2017b)

† Stations with sub-hourly and hourly records used for developing empirical relationship between erosivity values from coarser resolution rainfall and those from finer resolution data.
‡ Station density (km^2/station) is the study area divided by the number of stations used for the interpolation; gridded data are given in units of resolution.
§ The temporal resolution of rainfall data used for at-site (for the station data) or gridded (for the gridded data) *R* factor computation or the type of covariates (for the gridded covariates).
¶ NA, information is inaccessible from the references.

annual rainfall, bioclimatic variables, and topography information were usually used as covariates.

This overview suggests that future work on rainfall erosivity should give priority to the following aspects: the snowmelt and thaw effect on erosion; the parameters of daily erosivity estimation models for various climate zones; uncertainty evaluation of the erosivity maps; updated erosivity maps echoing the changing climate; and downscaling the general circulation model output for future assessment of the climate change impact on rainfall erosivity and soil erosion.

Acknowledgments

This work was supported by the project supported by State Key Laboratory of Earth Surface Processes and Resource Ecology, the China Special Fund for Meteorological Research in the Public Interest (GYHY201506014), and the USDA–ARS.

References

Agnese, C., V. Bagarello, C. Corrao, L. D'Agostino, and F. D'Asaro. 2006. Influence of the rainfall measurement interval on the erosivity determinations in the Mediterranean area. J. Hydrol. 329:39–48. doi:10.1016/j.jhydrol.2006.02.002

Angulo-Martínez, M., and S. Beguería. 2009. Estimating rainfall erosivity from daily precipitation records: A comparison among methods using data from the Ebro Basin (NE Spain). J. Hydrol. 379:111–121. doi:10.1016/j.jhydrol.2009.09.051

Angulo-Martínez, M., and S. Beguería. 2012. Trends in rainfall erosivity in NE Spain at annual, seasonal and daily scales, 1955–2006. Hydrol. Earth Syst. Sci. 9:6285–6309. doi:10.5194/hessd-9-6285-2012

Aronica, G., and V. Ferro. 1997. Rainfall erosivity over the Calabrian region. Hydrol. Sci. J. 42:35–48. doi:10.1080/02626669709492004

Ballabio, C., P. Borrelli, J. Spinoni, K. Meusburger, S. Michaelides, S. Beguería, and S. Aalto. 2017. Mapping monthly rainfall erosivity in Europe. Sci. Total Environ. 579:1298–1315. doi:10.1016/j.scitotenv.2016.11.123

Beguería, S., S.M. Vicente-Serrano, J.I. López-Moreno, and J.M. García-Ruiz. 2009. Annual and seasonal mapping of peak intensity, magnitude and duration of extreme precipitation events across a climatic gradient, northeast Spain. Int. J. Climatol. 29:1759–1779. doi:10.1002/joc.1808

Bennett, H.H. 1939. Soil conservation. McGraw-Hill, New York.

Bonilla, C.A., and K.L. Vidal. 2011. Rainfall erosivity in central Chile. J. Hydrol. 410:126–133. doi:10.1016/j.jhydrol.2011.09.022

Borrelli, P., N. Diodato, and P. Panagos. 2016. Rainfall erosivity in Italy: A national scale spatio-temporal assessment. Int. J. Digital Earth 9:835–850. doi:10.1080/17538947.2016.1148203

Brown, L.C., and G.R. Foster. 1987. Storm erosivity using idealized intensity distributions. Trans. ASAE 30:379–386. doi:10.13031/2013.31957

Browning, G.M., C.L. Parish, and J. Glass. 1947. A method for determining the use and limitation of rotation and conservation practices in control of soil erosion in Iowa. J. Am. Soc. Agron. 39:65–73. doi:10.2134/agronj1947.00021962003900010008x

Capolongo, D., N. Diodato, C.M. Mannaerts, and M. Piccarreta. 2008. Analyzing temporal changes in climate erosivity using a simplified rainfall erosivity model in Basilicata (southern Italy). J. Hydrol. 356:119–130. doi:10.1016/j.jhydrol.2008.04.002

Carter, C.E., J.D. Greer, H.J. Braud, and J.M. Floyd. 1974. Raindrop characteristics in south central United States. Trans. ASABE 17:1033–1037. doi:10.13031/2013.37021

Catari, G., J. Latron, and F. Gallart. 2011. Assessing the sources of uncertainty associated with the calculation of rainfall kinetic energy and erosivity: Application to the Upper Llobregat basin, NE Spain. Hydrol. Earth Syst. Sci. 15:679–688. doi:10.5194/hess-15-679-2011

Cooley, K.R., C.L. Hanson, and C.W. Johnson. 1988. Precipitation erosivity index estimates in cold climates. Trans. ASAE 31:1445–1450. doi:10.13031/2013.30883

Daly, C., G. Taylor, and W. Gibson. 1997. The PRISM approach to mapping precipitation and temperature. In: Proceedings of the 10th Conference on Applied Climatology, Reno, NV. 20–24 Oct. 1997. Am. Meteorol. Soc., Boston. p. 20–23.

Diodato, N., and G. Bellocchi. 2009. Assessing and modelling changes in rainfall erosivity at different climate scales. Earth Surf. Processes Landforms 34:969–980. doi:10.1002/esp.1784

Diodato, N., G. Verstraeten, and G. Bellocchi. 2014. Decadal modelling of rainfall erosivity in Belgium. Land Degrad. Dev. 25:511–519. doi:10.1002/ldr.2168

Eltaif, N.I., M.A. Gharaibeh, F. Al-Zaitawi, and M.N. Alhamad. 2010. Approximation of rainfall erosivity factors in North Jordan. Pedosphere 20:711–717. doi:10.1016/S1002-0160(10)60061-6

Fagnano, M., N. Diodato, I. Alberico, and N. Fiorentino. 2012. An overview of soil erosion modelling compatible with RUSLE approach. Rendiconti Lincei 23:9–80. doi:10.1007/s12210-011-0159-8

Fan, J.R., and C. Yang. 2013. Characteristics of rainfall erosivity based on tropical rainfall measuring mission data in Tibet, China. J. Mountain Sci. 10:1008–1017.

FAO. 2015. Status of the world's soil resources. Main report. FAO, Rome.

Ferro, V., G. Giordano, and M. Iovino. 1991. Isoerosivity and erosion risk map for Sicily. Hydrol. Sci. J. 36:549–564. doi:10.1080/02626669109492543

Fiener, P., P. Neuhaus, and J. Botschek. 2013. Long-term trends in rainfall erosivity: Analysis of high resolution precipitation time series (1937–2007) from western Germany. Agric. For. Meteorol. 171-172:115–123. doi:10.1016/j.agrformet.2012.11.011

Fornis, R.L., H.R. Vermeulen, and J.D. Nieuwenhuis. 2005. Kinetic energy–rainfall relationship for central Cebu, Philippines for soil erosion. J. Hydrol. 300:20–32. doi:10.1016/j.jhydrol.2004.04.027

Goovaerts, P. 1999. Using elevation to aid the geostatistical mapping of rainfall erosivity. Catena 34:227–242. doi:10.1016/S0341-8162(98)00116-7

Grauso, S., N. Diodato, and V. Verrubbi. 2010. Calibrating a rainfall erosivity assessment model at regional scale in Mediterranean area. Environ. Earth Sci. 60:1597–1606. doi:10.1007/s12665-009-0294-z

Hanel, M., P. Maca, P. Basta, R. Vlnas, and P. Pech. 2016. The rainfall erosivity factor in the Czech Republic and its uncertainty. Hydrol. Earth Syst. Sci. 20:4307–4322. doi:10.5194/hess-20-4307-2016

Hijmans, R.J., S.E. Cameron, J.L. Parra, P.G. Jones, and A. Jarvis. 2005. Very high resolution interpolated climate surfaces for global land areas. Int. J. Climatol. 25:1965–1978. doi:10.1002/joc.1276

Hollinger, S.E., J.R. Angel, and M.A. Palecki. 2002. Spatial distribution, variation, and trends in storm precipitation characteristics associated with soil erosion in the United States. Illinois State Water Surv. Contract Rep. 99. Univ. of Illinois, Champaign.

Hoyos, N., P.R. Waylen, and Á. Jaramillo. 2005. Seasonal and spatial patterns of erosivity in a tropical watershed of the Colombian Andes. J. Hydrol. 314:177–191. doi:10.1016/j.jhydrol.2005.03.014

Hudson, N.W. 1963. Raindrop size distribution in high intensity storms. Rhod. J. Agric. Res. 1:6–11.

IPCC. 2013. Climate change 2013: The physical science basis. Contribution of Working Group I to the Fifth Assessment Report of the Intergovernmental Panel on Climate Change. Cambridge Univ. Press, Cambridge, UK.

Karydas, C.G., O. Tzoraki, and P. Panagos. 2015. A new spatiotemporal risk index for heavy metals: Application in Cyprus. Water 7:4323–4342. doi:10.3390/w7084323

Kinnell, P.I.A. 1981. Rainfall intensity–kinetic energy relationships for soil loss prediction. Soil Sci. Soc. Am. J. 45:153–155. doi:10.2136/sssaj1981.03615995004500010033x

Klik, A., K. Haas, A. Dvorackova, and I.C. Fuller. 2015. Spatial and temporal distribution of rainfall erosivity in New Zealand. Soil Res. 53:815–825. doi:10.1071/SR14363

Klik, A., and F. Konecny. 2013. Rainfall erosivity in northeastern Austria. Trans. ASABE 56:719–725. doi:10.13031/2013.42677

Krása, J., H. Středová, T. Dostál, and I. Novotný. 2014. Rainfall erosivity research on the territory of the Czech Republic. In: J. Rožnovský, and T. Litschmann, editors, Mendel a bioklimatologie. Mendel Univ., Brno, Czech Republic.

Laceby, J.P., C. Chartin, O. Evrard, Y. Onda, L. Garcia-Sanchez, and O. Cerdan. 2016. Rainfall erosivity in catchments contaminated with fallout from the Fukushima Daiichi nuclear power plant accident. Hydrol. Earth Syst. Sci. 20:2467–2482. doi:10.5194/hess-20-2467-2016

Laws, J.O., and D.A. Parsons. 1943. The relation of raindrop-size to intensity. Eos Trans. AGU 24:452–460. doi:10.1029/TR024i002p00452

Lee, M.H., and H.H. Lin. 2015. Evaluation of annual rainfall erosivity index based on daily, monthly, and annual precipitation data of rainfall station. Int. J. Distrib. Sensor Networks 2015:2–15. doi:10.1155/2015/214708

Liu, B.Y., S.Y. Guo, Z.G. Li, Y. Xie, K.L. Zhang, and X.C. Liu. 2013. Sample survey on water erosion in China. (In Chinese with English abstract.) Soil Water Conserv. China 10:26–34.

Lu, H., and B. Yu. 2002. Spatial and seasonal distribution of rainfall erosivity in Australia. Soil Res. 40:887–901. doi:10.1071/SR01117

Ma, X., Y. He, J. Xu, M. van Noordwijk, and X. Lu. 2014. Spatial and temporal variation in rainfall erosivity in a Himalayan watershed. Catena 121:248–259. doi:10.1016/j.catena.2014.05.017

McCool, D.K., M.T. Walter, and L.G. King. 1995. Runoff index values for frozen soil areas of the Pacific Northwest. J. Soil Water Conserv. 50:466–469.

McGregor, K.C., R.L. Bingner, A.J. Bowie, and G.R. Foster. 1995. Erosivity index values for northern Mississippi. Trans. ASAE 38:1039–1047. doi:10.13031/2013.27921

McGregor, K.C., and C.K. Mutchler. 1976. Status of the *R* factor in northern Mississippi. In: C.R. Forster, editor, Soil erosion: Prediction and control. Spec. Publ. 21. Soil Conserv. Soc. Am., Ankeny, IA. p. 135–142.

Meddi, M., S. Toumi, and A.A. Assani. 2016. Spatial and temporal variability of the rainfall erosivity factor in northern Algeria. Arab. J. Geosci. 9:282. doi:10.1007/s12517-015-2303-8

Mello, C.D., M.R. Viola, S. Beskow, and L.D. Norton. 2013. Multivariate models for annual rainfall erosivity in Brazil. Geoderma 202:88–102. doi:10.1016/j.geoderma.2013.03.009

Men, M., Z. Yu, and H. Xu. 2008. Study on the spatial pattern of rainfall erosivity based on geostatistics in Hebei Province, China. Front. Agric. China 2:281–289. doi:10.1007/s11703-008-0042-2

Meusburger, K., A. Steel, P. Panagos, L. Montanarella, and C. Alewell. 2012. Spatial and temporal variability of rainfall erosivity factor for Switzerland. Hydrol. Earth Syst. Sci. 16:167–177. doi:10.5194/hess-16-167-2012

Mezősi, G., and T. Bata. 2016. Estimation of the changes in the rainfall erosivity in Hungary. J. Environ. Geogr. 9:43–48. doi:10.1515/jengeo-2016-0011

Mikhailova, E.A., R.B. Bryant, S.J. Schwager, and S.D. Smith. 1997. Predicting rainfall erosivity in Honduras. Soil Sci. Soc. Am. J. 61:273–279. doi:10.2136/sssaj1997.03615995006100010039x

Millward, A.A., and J.E. Mersey. 1999. Adapting the RUSLE to model soil erosion potential in a mountainous tropical watershed. Catena 38:109–129. doi:10.1016/S0341-8162(99)00067-3

Moses, A.N. 2017. Spatial variation of rainfall runoff erosivity (*R*) factor for River Nzoia basin, western Kenya. Int. J. Civ. Eng. Technol. 8:418–422.

Musgrave, G.W. 1947. The quantitative evaluation of factors in water erosion, a first approximation. J. Soil Water Conserv. 2(3):133–138.

Naipal V., C. Reick, J. Pongratz, and K. Van Oost. 2015. Improving the global applicability of the RUSLE model: Adjustment of the topographical and rainfall erosivity factors. Geosci. Model Dev. 8:2893–2913. doi:10.5194/gmd-8-2893-2015

Nearing, M.A. 2001. Potential changes in rainfall erosivity in the U.S. with climate change during the 21st century. J. Soil Water Conserv. 56:229–232.

Nearing, M.A., C.L. Unkrich, D.C. Goodrich, M.H. Nichols, and T.O. Keefer. 2015. Temporal and elevation trends in rainfall erosivity on a 149 km^2 watershed in a semi-arid region of the American Southwest. Int. Soil Water Conserv. Res. 3:77–85. doi:10.1016/j.iswcr.2015.06.008

Nearing, M.A., S. Yin, P. Borrelli, and V.O. Polyakov. 2017. Rainfall erosivity: An historical review. Catena 157:357–362. doi:10.1016/j.catena.2017.06.004

Norzagaray-Campos, M., P. Muñoz-Sevilla, L. Espinosa-Carreón, R. Ruíz-Guerrero, H. González-Ocampo, and O. Llanes-Cárdenas. 2016. Erosivity indicators based on rainfall in northwestern Mexico. J. Environ. Eng. Landscape Manage. 24:133–142. doi:10.3846/16486897.2015.1106405

Oliveira, P.T.S., D.B.B, Rodrigues, T.A. Sobrinho, D.F. de Carvalho, and E. Panachuki. 2012a. Spatial variability of the rainfall erosive potential in the state of Mato Grosso do Sul, Brazil. Eng. Agric. 32:69–79. doi:10.1590/S0100-69162012000100008

Oliveira, P.T.S., E. Wendland, and M.A. Nearing. 2012b. Rainfall erosivity in Brazil: A review. Catena 100:139–147. doi:10.1016/j.catena.2012.08.006

Onaga, K., K. Shirai, and A. Yoshinaga. 1988. Rainfall erosion and how to control its effects on farmland in Okinawa. In: S. Rimwanich, editor, Land conservation for future generations. Dep. Land Dev., Bangkok. p. 627–639.

Panagos, P., C. Ballabio, P. Borrelli, and K. Meusburger. 2016a. Spatiotemporal analysis of rainfall erosivity and erosivity density in Greece. Catena 137:161–172. doi:10.1016/j.catena.2015.09.015

Panagos, P., C. Ballabio, P. Borrelli, K. Meusburger, A. Klik, S. Rousseva, and C. Alewell. 2015. Rainfall erosivity in Europe. Sci. Total Environ. 511:801–814. doi:10.1016/j.scitotenv.2015.01.008

Panagos, P., C. Ballabio, K. Meusburger, J. Spinoni, C. Alewell, and P. Borrelli. 2017a. Towards estimates of future rainfall erosivity in Europe

based on REDES and WorldClim datasets. J. Hydrol. 548:251–262. doi:10.1016/j.jhydrol.2017.03.006

Panagos, P., P. Borrelli, K. Meusburger, B. Yu, A. Klik, K.J. Lim, et al. 2017b. Global rainfall erosivity assessment based on high-temporal resolution rainfall records. Sci. Rep. 7:4175. doi:10.1038/s41598-017-04282-8

Panagos, P., P. Borrelli, J. Spinoni, C. Ballabio, K. Meusburger, S. Beguería, et al. 2016b. Monthly rainfall erosivity: Conversion factors for different time resolutions and regional assessments. Water 8(4):119. doi:10.3390/w8040119

Porto, P. 2016. Exploring the effect of different time resolutions to calculate the rainfall erosivity factor *R* in Calabria, southern Italy. Hydrol. Process. 30:1551–1562. doi:10.1002/hyp.10737

Qin, W., Q. Guo, C. Zuo, Z. Shan, L. Ma, and G. Sun. 2016. Spatial distribution and temporal trends of rainfall erosivity in mainland China for 1951–2010. Catena 147:177–186. doi:10.1016/j.catena.2016.07.006

Ramos, M.C., and B. Duran. 2014. Assessment of rainfall erosivity and its spatial and temporal variabilities: Case study of the Penedès area (NE Spain). Catena 123:135–147. doi:10.1016/j.catena.2014.07.015

Renard, K.G., G.R. Foster, G.A. Weesies, D.K. Mc Cool, and D.C. Yoder. 1997. Predicting rainfall erosion by water: A guide to conservation planning with the Revised Universal Soil Loss Equation (RUSLE). Agric. Handb. 703. US Gov. Print. Office, Washington, DC.

Richardson, C.W., G.R. Foster, and D.A. Wright. 1983. Estimation of erosion index from daily rainfall amount. Trans. ASAE 26:153–156.

Risal, A., R. Bhattarai, D. Kum, Y.S. Park, J.E. Yang, and K.J. Lim. 2016. Application of Web ERosivity Module (WERM) for estimation of annual and monthly *R* factor in Korea. Catena 147:225–237. doi:10.1016/j.catena.2016.07.017

Rosewell, C.J. 1986. Rainfall kinetic energy in eastern Australia. J. Clim. Appl. Meteorol. 25:1695–1701. doi:10.1175/1520-0450(1986)025<1695:RKEIEA>2.0.CO;2

Sadeghi, S.H.R., M. Moatamednia, and M. Behzadfar. 2011. Spatial and temporal variations in the rainfall erosivity factor in Iran. J. Agric. Sci. Technol. 13:451–464.

Sadeghi, S.H.R., M. Zabihi, M. Vafakhah, and Z. Hazbavi. 2017. Spatiotemporal mapping of rainfall erosivity index for different return periods in Iran. Nat. Hazards 87:35–56. doi:10.1007/s11069-017-2752-3

Salako, F.K. 2010. Development of isoerodent maps for Nigeria from daily rainfall amount. Geoderma 156:372–378. doi:10.1016/j.geoderma.2010.03.006

Schmidt, S., C. Alewell, P. Panagos, and K. Meusburger. 2016. Regionalization of monthly rainfall erosivity patterns in Switzerland. Hydrol. Earth Syst. Sci. 20:4359–4373. doi:10.5194/hess-20-4359-2016

Segura, C., G. Sun, S. McNulty, and Y. Zhang. 2014. Potential impacts of climate change on soil erosion vulnerability across the conterminous United States. J. Soil Water Conserv. 69:171–181. doi:10.2489/jswc.69.2.171

Shamshad, A., M.N. Azhari, M.A. Isa, W.W. Hussin, and B.P. Parida. 2008. Development of an appropriate procedure for estimation of RUSLE EI_{30} index and preparation of erosivity maps for Pulau Penang in Peninsular Malaysia. Catena 72:423–432. doi:10.1016/j.catena.2007.08.002

Shiono, T., S. Ogawa, T. Miyamoto, and K. Kameyama. 2013. Expected impacts of climate change on rainfall erosivity of farmlands in Japan. Ecol. Eng. 61:678–689. doi:10.1016/j.ecoleng.2013.03.002

Smith, D.D. 1941. Interpretation of soil conservation data for field use. Agric. Eng. 22:173–175.

Toreti, A., P. Naveau, M. Zampieri, A. Schindler, E. Scoccimarro, E. Xoplaki, et al. 2013. Projections of global changes in precipitation extremes from Coupled Model Intercomparison Project Phase 5 models. Geophys. Res. Lett. 40:4887–4892. doi:10.1002/grl.50940

USDA–ARS. 2013. Science documentation: Revised Universal Soil Loss Equation Version 2. USDA–ARS, Washington, DC.

Van der Knijff, J.M.F., R.J.A. Jones, and L. Montanarella. 1999. Soil erosion risk assessment in Italy. Joint Research Centre of the European Commission, Brussels.

van Dijk, A.I.J.M., L.A. Bruijnzeel, and C.J. Rosewell. 2002. Rainfall intensity–kinetic energy relationships: A critical literature appraisal. J. Hydrol. 261:1–23. doi:10.1016/S0022-1694(02)00020-3

Van Doren, C.A., and L.J. Bartelli. 1956. A method of forecasting soil losses. Agric. Eng. 37:335–341.

Verstraeten, G., and J. Poesen. 2006. Long-term (105 years) variability in rain erosivity as derived from 10-min rainfall depth data for Ukkel (Brussels, Belgium): Implications for assessing soil erosion rates. J. Geophys. Res. 111:D22109. doi:10.1029/2006JD007169

Vrieling, A., J.C.B. Hoedjes, and M.V.D. Velde. 2014. Towards large-scale monitoring of soil erosion in Africa: Accounting for the dynamics of rainfall erosivity. Global Planet. Change 115:33–43. doi:10.1016/j.gloplacha.2014.01.009

Vrieling, A., G. Sterk, and S.M. de Jong. 2010. Satellite-based estimation of rainfall erosivity for Africa. J. Hydrol. 395:235–241. doi:10.1016/j.jhydrol.2010.10.035

Wang, Y., C. Cheng, Y. Xie, B. Liu, S. Yin, Y. Liu, and Y. Hao. 2017. Increasing trends in rainfall–runoff erosivity in the source region of the Three Rivers, 1961–2012. Sci. Total Environ. 592:639–648. doi:10.1016/j.scitotenv.2017.02.235

Weiss, L.L. 1964. Ratio of true to fixed-interval maximum rainfall. J. Hydraul. Div. Am. Soc. Civ. Eng. 90:7–82.

Wischmeier, W.H. 1959. A rainfall erosion index for a universal soil-loss equation. Soil Sci. Soc. Am. Proc. 23:246–249. doi:10.2136/sssaj1959.03615995002300030027x

Wischmeier, W.H. 1962. Rainfall erosion potential: Geographic and location differences of distribution. Agric. Eng. 43:212–215, 225.

Wischmeier, W.H., and D.D. Smith. 1958. Rainfall energy and its relationship to soil loss. Trans. Am. Geophys. Union 39(2):285–291. doi:10.1029/TR039i002p00285

Wischmeier, W.H., and D.D. Smith. 1965. Predicting rainfall erosion losses in the Eastern U.S.: A guide to conservation planning. Agric. Handb. 282. US Gov. Print. Office, Washington, DC.

Wischmeier, W.H., and D.D. Smith. 1978. Predicting rainfall erosion losses: A guide to conservation planning. Agric. Handb. 537. US Gov. Print. Office, Washington, DC.

Xie, Y., B. Liu, and M.A. Nearing. 2002. Practical thresholds for separating erosive and non-erosive storms. Trans. ASABE 45:1843–1847.

Xie, Y., S. Yin, B. Liu, M.A. Nearing, and Y. Zhao. 2016. Models for estimating daily rainfall erosivity in China. J. Hydrol. 535:547–558. doi:10.1016/j.jhydrol.2016.02.020

Xin, Z., X. Yu, Q. Li, and X.X. Lu. 2011. Spatiotemporal variation in rainfall erosivity on the Chinese Loess Plateau during the period 1956–2008. Reg. Environ. Change 11:149–159. doi:10.1007/s10113-010-0127-3

Yang, F., and C. Lu. 2015. Spatiotemporal variation and trends in rainfall erosivity in China's dryland region during 1961–2012. Catena 133:362–372. doi:10.1016/j.catena.2015.06.005

Yang, X., and B. Yu. 2015. Modelling and mapping rainfall erosivity in New South Wales, Australia. Soil Res. 53:178–189.

Yang, X., B. Yu, and X. Xie. 2015. Predicting changes of rainfall erosivity and hillslope erosion risk across greater Sydney region, Australia. Int. J. Geospatial Environ. Res. 2(1):2. http://dc.uwm.edu/ijger/vol2/iss1/2 (accessed 30 Oct. 2017).

Yin, S., Y. Xie, B. Liu, and M.A. Nearing. 2015. Rainfall erosivity estimation based on rainfall data collected over a range of temporal resolutions. Hydrol. Earth Syst. Sci. 12:4965–4996. doi:10.5194/hessd-12-4965-2015

Yin, S., Y. Xie, M.A. Nearing, and C. Wang. 2007. Estimation of rainfall erosivity using 5- to 60-minute fixed-interval rainfall data from China. Catena 70:306–312. doi:10.1016/j.catena.2006.10.011

Yin, S., W. Zhang, Y. Xie, S. Liu, and F. Liu. 2013. Spatial distribution of rainfall erosivity over China based on high-density daily precipitation stations. (In Chinese.) Soil Water Conserv. China 10:45–51.

Yu, B. 1998. Rainfall erosivity and its estimation for Australia's tropics. Aust. J. Soil Res. 36:143–165. doi:10.1071/S97025

Yu, B. 1999. A comparison of the *R*-factor in the Universal Soil Loss Equation and Revised Universal Soil Loss Equation. Trans. ASAE 42:1615–1620. doi:10.13031/2013.13327

Yu, B., G.M. Hashim, and Z. Eusof. 2001. Estimating the *R*-factor with limited rainfall data: A case study from Peninsular Malaysia. J. Soil Water Conserv. 56(2):101–105.

Yu, B., and C.J. Rosewell. 1996. Rainfall erosivity estimation using daily rainfall amounts for South Australia. Aust. J. Soil Res. 34:721–733. doi:10.1071/SR9960721

Zhang, Y., M. Hernandez, E. Anson, and M.A. Nearing. 2012. Modeling climate change effects on runoff and erosion in southeastern Arizona rangelands and mitigation with traditional rangeland conservation practices. J. Soil Water Conserv. 67:390–405. doi:10.2489/jswc.67.5.390

Zhang, Y., M.A. Nearing, X.C. Zhang, Y. Xie, and H. Wei. 2010. Projected rainfall erosivity changes under climate change from multimodel and multiscenario projections in Northeast China. J. Hydrol. 384:97–106. doi:10.1016/j.jhydrol.2010.01.013

Zhu, Z., and B. Yu. 2015. Validation of rainfall erosivity estimators for mainland China. Trans. ASABE 58:61–71.

Zingg, R.W. 1940. Degree and length of land slope as it affects soil loss in runoff. Agric. Eng. 21:59–64.